SROC: Space Rider Observer Cube Mission

Medical Engineering and Physics 114 (2023) 103967

Contents lists available at ScienceDirect

Medical Engineering and Physics

journal homepage: www.elsevier.com/locate/medengphy

A computational analysis of a novel therapeutic approach combining an advanced medicinal therapeutic device and a fracture fixation assembly for the treatment of osteoporotic fractures: Effects of physiological loading, interface conditions, and fracture fixation materials

Subrata Mondal [a], David B. MacManus [a,b], Amedeo Franco Bonatti [j,k], Carmelo De Maria [j,k], Kenny Dalgarno [l], Maria Chatzinikolaidou [m,n], Aurora De Acutis [j,k], Giovanni Vozzi [j,k], Sonia Fiorilli [o], Chiara Vitale-Brovarone [o], Nicholas Dunne [a,b,c,d,e,f,g,h,i,*]

[a] School of Mechanical and Manufacturing Engineering, Dublin City University, Ireland
[b] Centre for Medical Engineering Research, Dublin City University, Ireland
[c] School of Pharmacy, Queen's University Belfast, Belfast BT9 7BL, United Kingdom
[d] Department of Mechanical and Manufacturing Engineering, School of Engineering, Trinity College Dublin, Dublin 2, Ireland
[e] Advanced Manufacturing Research Centre (I-Form), School of Mechanical and Manufacturing Engineering, Dublin City University, Dublin 9, Ireland
[f] Advanced Materials and Bioengineering Research Centre (AMBER), Trinity College Dublin, Dublin 2, Ireland
[g] Trinity Centre for Biomedical Engineering, Trinity Biomedical Sciences Institute, Trinity College Dublin, Dublin 2, Ireland
[h] Advanced Processing Technology Research Centre, Dublin City University, Dublin 9, Ireland
[i] Biodesign Europe, Dublin City University, Dublin 9, Ireland
[j] Research Center E. Piaggio, University of Pisa, Largo Lucio Lazzarino 1, Pisa, Italy
[k] Department of Information Engineering, University of Pisa, Via G. Caruso 16, Pisa, Italy
[l] School of Engineering, Newcastle University, Newcastle upon Tyne NE1 7RU, UK
[m] Department of Materials Science and Technology, University of Crete, Heraklion, Greece
[n] Institute of Electronic Structure and Laser, Foundation for Research and Technology-Hellas, Heraklion, Greece
[o] Department of Applied Science and Technology, Politecnico di Torino, Italy

ARTICLE INFO

Keywords:
Periprosthetic femoral fracture
Osteoporosis
Bone regeneration
Finite element analysis
Femur
Fracture fixation assembly

ABSTRACT

The occurrence of periprosthetic femoral fractures (PFF) has increased in people with osteoporosis due to decreased bone density, poor bone quality, and stress shielding from prosthetic implants. PFF treatment in the elderly is a genuine concern for orthopaedic surgeons as no effective solution currently exists. Therefore, the goal of this study was to determine whether the design of a novel advanced medicinal therapeutic device (AMTD) manufactured from a polymeric blend in combination with a fracture fixation plate in the femur is capable of withstanding physiological loads without failure during the bone regenerative process. This was achieved by developing a finite element (FE) model of the AMTD together with a fracture fixation assembly, and a femur with an implanted femoral stem. The response of both normal and osteoporotic bone was investigated by implementing their respective material properties in the model. Physiological loading simulating the peak load during standing, walking, and stair climbing was investigated. The results showed that the fixation assembly was the prime load bearing component for this configuration of devices. Within the fixation assembly, the bone screws were found to have the highest stresses in the fixation assembly for all the loading conditions. Whereas the stresses within the AMTD were significantly below the maximum yield strength of the device's polymeric blend material. Furthermore, this study also investigated the performance of different fixation assembly materials and found Ti-6Al-4V to be the optimal material choice from those included in this study.

* Corresponding author.
E-mail address: nicholas.dunne@dcu.ie (N. Dunne).

https://doi.org/10.1016/j.medengphy.2023.103967
Received 8 June 2022; Received in revised form 13 February 2023; Accepted 8 March 2023
Available online 12 March 2023

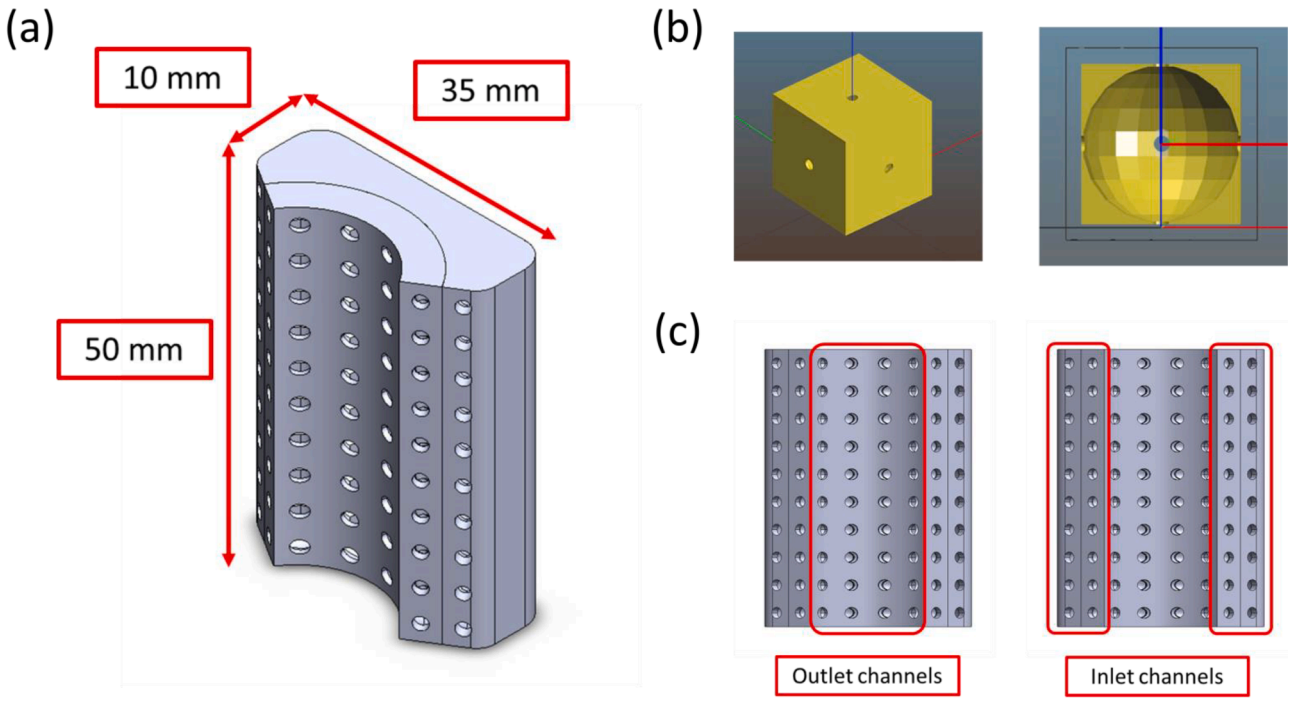

Fig. 1. In (a) a general view of the device alongside the overall dimensions. In (b), the basic porous unit that is repeated in the 3D space to obtain the final device shape. In (c), visualization of the channels that direct diffusion to the fracture (outlet channels) and can be used to fill the device with a drug-loaded hydrogel (inlet channels).

1. Introduction

Osteoporosis is a significant socio-economic problem with an estimated 200 million people worldwide that are affected by this disease [1]. The statistics from the international osteoporosis foundation states that 33-50% of women and 20% of men over fifty years have osteoporosis [2]. Periprosthetic femoral fractures (PFF) are the third most common reason for an implant revision in people with osteoporosis [3]. PFF may occur due to osteoporotic-induced decrease in bone strength and bone quality, in combination with implant-induced stress shielding further exacerbating bone quality and strength. In elderly people with a total hip replacement, PFF are becoming more frequent and increasingly difficult to treat [4] with up to 18% of total hip arthroplasty (THA) resulting in postoperative periprosthetic fracture [5]. Furthermore, Draw *et al.* reported mortality rates of 13.1% and 15.8% at 12 and 18 months following treatment for PFF [6], and Bhattacharya *et al.* found an 11% mortality rate in people treated for PFF after 12 months. Several studies have suggested there is a high rate of bone failure and mortality for PFF [7]. The treatment for PFF in the elderly is a genuine concern for orthopaedic surgeons as no effective solution is currently available on the market. Furthermore, there is no gold standard for PFF treatment despite numerous randomised clinical trials on external and internal fracture fixation devices [8]. However, tissue engineering and regenerative medicine has shown significant potential in its ability to repair bone defects resulting from PFF and osteoporotic fractures [9]. Devices such as tissue-engineered (TE) scaffolds are generally used to fill the defects, stimulate bone tissue growth, and replace the diseased bone with the newly formed healthy bone [10]. Porous TE scaffolds provide a suitable substrate for cells to attach, migrate and proliferate within to support tissue growth under a suitable physiological bone environment. Porous bone TE scaffolds stimulate cell proliferation and differentiation and bears the necessary mechanical load [11]. However, for elderly people with osteoporotic PFF, the surgical implantation of a porous bone TE scaffold is a challenging task for an orthopaedic surgeon. As an alternative solution, the overall goal of the research programme is focussed on developing a new advanced medicinal therapeutic device (AMTD) that has the ability to be fixed across fracture sites to treat PFF in long bones. This alternative therapeutic strategy can be used in conjunction with an existing fracture fixation assembly and overcome the complexities associated with the implantation of a novel medical device.

Computational modelling is a widely used technique for studying biomechanics and medical device design [12] and is well suited for investigating the biomechanics of novel devices to treat osteoporotic PFF. It has been effectively used to control the different design parameters related to the medical device, fixation, failure, and performance analysis in bone biomechanics problems. Moreover, computational modelling can model complex geometrical structures with material behaviour, and efficiently simulate the complicated boundary and loading conditions present in device-tissue interactions. Furthermore, device geometry and material selection can be optimised during computational modelling prior to preclinical studies.

Therefore, the primary objective of this study is to quantify the effect of physiological loading on the mechanical stability and effectiveness of the fracture fixation assembly to direct damaging stresses away from a novel AMTD for bone regeneration in osteoporotic PFF. This was achieved by developing a finite element (FE) model of the AMTD that can be fixed across a fracture to guide and stimulate bone regeneration at the fracture site. The AMTD was integrated with an existing femur fracture fixation assembly, i.e., metallic fixation plates, bone screws and cerclage cables. The fixation assembly was used to support the AMTD. The AMTD was designed not to be load-bearing as it is assumed that all of the load will be transmitted through the fracture fixation devices. Therefore, the subsequent objectives of this study were to: (1) Predict the stress distributions through the AMTD, fixation assembly, femoral implant, and the femur during the peak physiological loading conditions demonstrating that the bulk of the load is transmitted through the fixation assembly; (2) study the effect of bone-AMTD, bone-cables, and bone-screws interface conditions on the stress distribution, and (3) investigate the failure strength of the AMTD under physiological loading conditions for both normal and osteoporotic bone. Additionally, the effectiveness of different fracture fixation assembly materials on

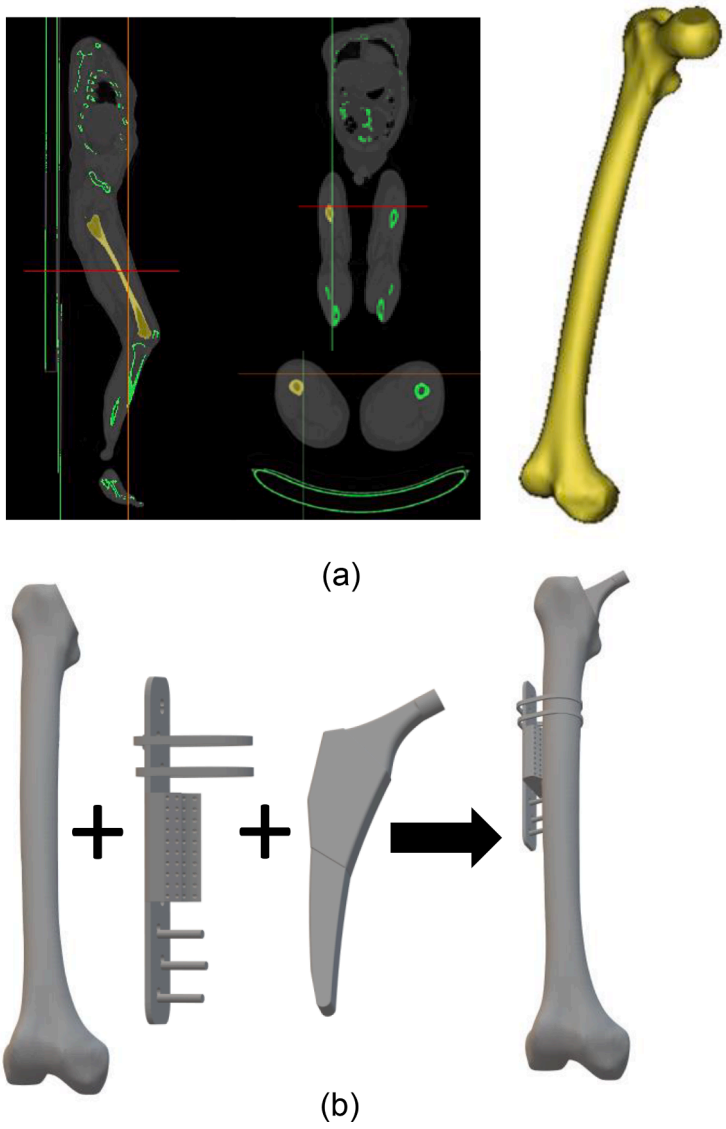

Fig. 2. (a) The generation of femur bone from CT data, and (b) virtual positioning and operation of the CAD files of fracture fixation assembly, femoral implant, and scaffold device with the femur bone.

Table 1
Material property data of the femoral bone, femoral implant, device and plate fixation assembly [16–23]. AMTD = Advanced medicinal therapeutic device.

Component	Young's Modulus (GPa)	Poisson's Ratio (υ)	References
Femoral Bone	17.26	0.3	[16]
Femoral Implant	230	0.26	[16]
AMTD	2.52	0.3	[17]
Candidate Materials for the Plate Fixation Assembly			
Alumina (Al_2O_3)	240	0.31	[18,20–22]
Cobalt Chrome (Co-Cr) alloy	210	0.30	[19,22,23]
Stainless Steel (SS316L) alloy	193	0.31	[20–22]
Titanium (Ti-6Al-4V) alloy	120	0.32	[20–22]

shielding the AMTD from damaging stresses was also investigated.

2. Materials and method

2.1. General overview of the advanced medicinal therapeutic device

The AMTD is in active development and is part of the European Union's Horizon 2020 Research and Innovation programme under grant agreement No 814410: Active aGeIng and Osteoporosis: The next challenge for smarT nanobiOmaterials and 3D technologies (GIOTTO). The specific objective of the H2020 GIOTTO project is to develop a novel advanced medicinal therapeutic device that combines the use of nanomaterials and an active molecule to stimulate fracture healing in long bones. In particular, the general design can be seen in Fig. 1 (a), alongside the device's dimensions. The main concept is to have controlled **delivery** of relevant ions and drugs towards the osteoporotic PFF to promote healing and regeneration . As such, the AMTD architecture was obtained by repeating a basic unit in three-dimensional (3D) space to create a porous structure with internally connected pores (Fig. 1 (b)). A porosity value of 50% was set for all repeated units, while the channels diameter was 1.5 mm. Ions and drugs can be included inside

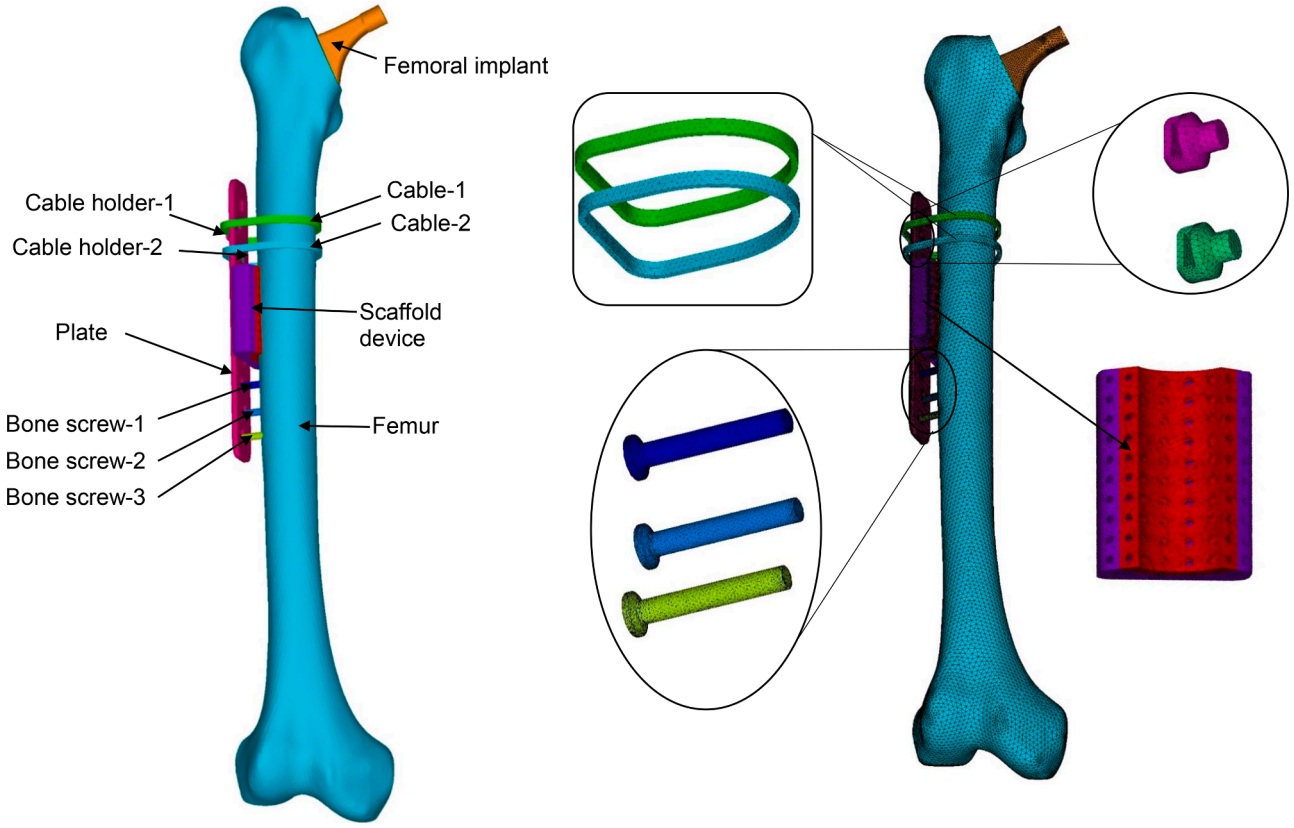

Fig. 3. FE model of femur bone with the fracture fixation assembly, femoral implant, and AMTD.

Table 2
Forces representing different body weights during standing posture that were applied to the femur bone under static loading conditions [16,27].

Load Case	Force
1	490 N
2	540 N
3	588 N
4	640 N
5	860 N

the device by grafting on the pore surface or by filling the device with an ion- or drug-loaded hydrogel (Fig. 1 (c)). The outer shape and overall dimensions of the device were chosen so that it could fit over the curved bone surface (so that at least 80% of the device is in contact with the tissue), while being able to integrate with existing bone fixation solutions, e.g., metallic plates, bone screws and cerclage cables. From a manufacturing point of view, the device is fabricated using Fused Deposition Modeling (FDM) of composite polymeric blends made of poly-L-lactic acid (PLLA), polycaprolactone (PCL), and poly (3-hydroxybutyrate-co-3-hydroxyvalerate) (PHBV). Moreover, the blend included an inorganic, ceramic phase comprising of nanohydroxyapatite (nHA) and/or mesoporous bioactive glasses (MBGs) with/without strontium doping, known to stimulate bone regeneration as previously reported [13].

The present paper demonstrates the general characteristics, design aspects, and mechanical function of the AMTD. A parametric computer design was utilised to determine the internal topology of the AMTD. Specifically, the internal topology was obtained as the repetition of a basic unit (Fig. 1 (a) and (b)). Channels were used to: (1) connect the central pores to create a pore network; and (2) direct diffusion towards the fracture (outlet channels in Fig. 1 (c)). The device was placed outside the bone and over the fracture, and in direct contact with the periosteum to enhance bone regeneration. The device should be non-load-bearing since other fixation devices will support the mechanical loads (i.e., metallic plate, bone screws, and cables).

2.2. Model generation

Computed tomography (CT) scan data of a 60 year old male (516 × 516 pixels, pixels size of 0.815 mm, and slice thickness of 1 mm) obtained from the Cancer Imaging Archive Database (National Cancer Institute, National Institutes of Health, Maryland, USA) was used to develop the 3D FE femur model for this study [14,15]. Manual segmentation, and 3D model generation of the femur bone was performed using MIMICS 24.0 (Materialise, Leuven, Belgium). The 3D geometry of the AMTD was generated using SolidWorks (DS SolidWorks Corp., Maryland, USA). Similarly, the 3D geometry of the fracture fixation assembly consisting of a plate, bone screws (1-3), cables (1-2), cable holders (1-2), and the femoral implant were created in SolidWorks (DS Solidworks Corp., Maryland, USA). The overall dimensions of the AMTD used for FE simulations can be seen in Fig. 1 (a).

Virtual positioning of the fracture fixation assembly, femoral implant and the AMTD with the femur bone was performed in Rhinoceros 7.0 (Robert McNeel & Associates, Washington, USA) (Fig. 2). All components were imported into ANSYS (ANSYS, Inc., Pennsylvania, USA) and a ten-node tetrahedral element mesh was used for the discretization process. The material property data for the femoral bone, fixation assembly and femoral implant are shown in Table 1 [16–23]. A Young's modulus of 2.52 GPa was determined for the AMTD following experimental mechanical characterisation [17]. The position of all the components of the FE model (i.e., femoral bone, femoral implant, plate, bone screws 1-3, cables 1-2, cable holders 1-2, and AMTD) are defined and shown in Fig. 3.

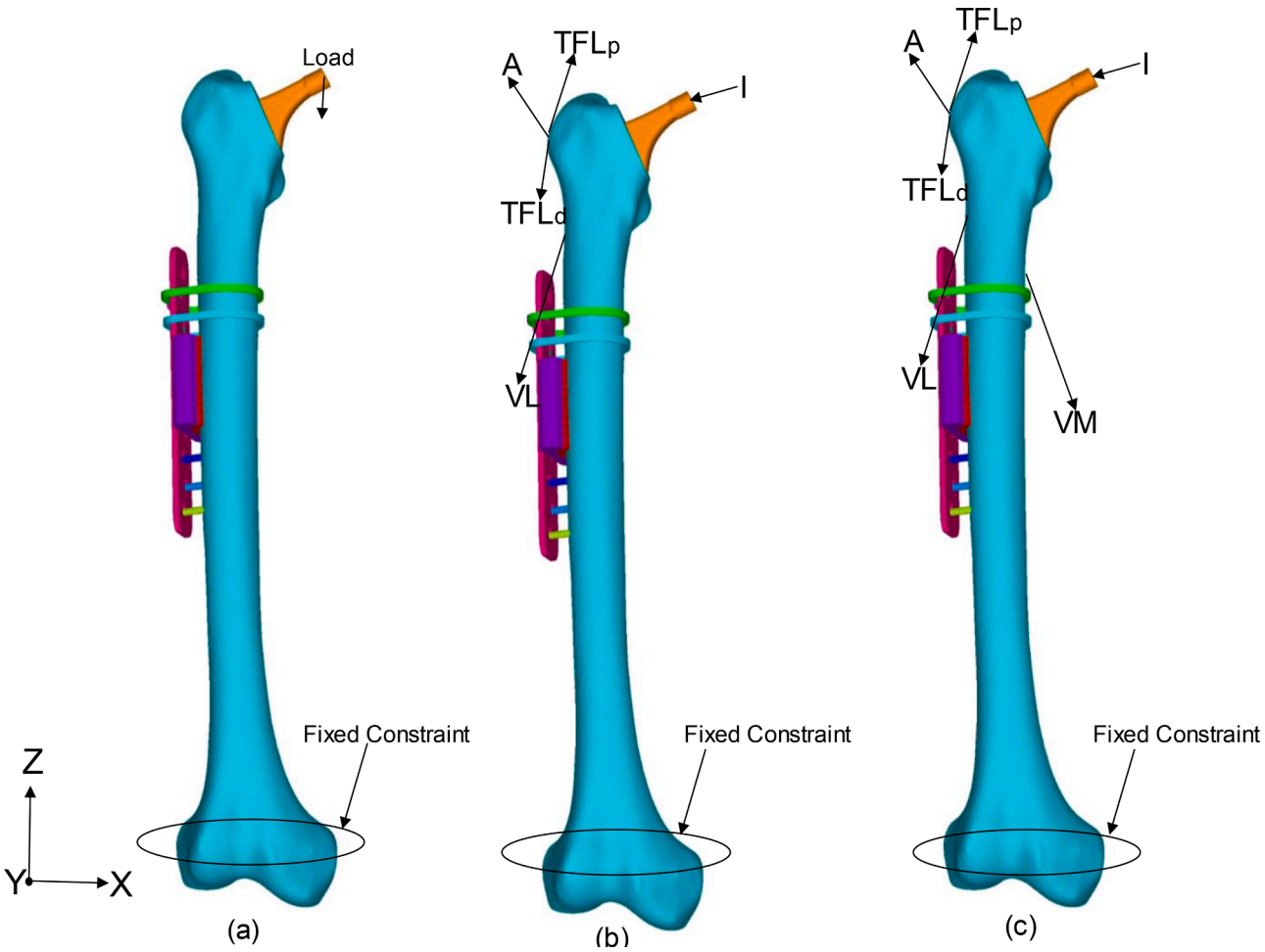

Fig. 4. Loading and boundary conditions at the FE model for (a) standing posture, (b) walking, and (c) stair climbing. (I: intersegmental joint muscle forces; A: abductor; TFL_p: tensor fascia latae proximal; TFL_d: tensor fascia latae distal; VL: vastus laterallis; VM: vastus medialis)

Table 3
The magnitude and direction of forces during walking and stair climbing condition when body weight = 860 N [16].

Force Components (N)	F_X	F_Y	F_Z
Walking			
I	17	-162	-1172
A	29	518	700
TFL_p	-87	70	113
TFL_d	-4	11	-159
VL	199	-34	-766
	Stair climbing		
I	142	-225	-1272
A	-174	639	706
TFL_p	-3	122	129
TFL_d	2	-15	-198
VL	257	-60	-1135
VM	-470	-158	-2245

2.3. Verification and validation of the FE model

A mesh convergence study was performed to verify the model. Four FE models were generated having different element sizes. The first, second, third and fourth FE models consisted of 535,867; 987,921; 1,214,268; and 1,567,822 elements, respectively. The equivalent stresses in the femoral bone, femoral implant, AMTD and fixation assembly were considered for the convergence study. The deviation in stresses was observed to be between 3% and 12% when the first and second FE models were compared. This deviation was reduced by 1-5% when a comparison was made between the second and third FE models. The comparison between the third and fourth FE models showed a significant reduction in the deviation of equivalent stresses in the range of 0.1–1%. Consequently, the third model consisting of 1,214,268 elements was sufficient for accurate computational modelling. The intact FE model of the femoral bone was validated with results from previously published data [19,24].

2.4. Modelling of osteoporotic bone

It is well established that osteoporosis is a risk factor for PFF [8]. Therefore, it is beneficial to use material property data for osteoporotic bone as well as for normal healthy bone when modelling the femur's response to the fracture fixation assembly under load. Osteoporosis leads to a reduction of bone quality and consequently its Young's modulus and density. Considering this effect, the material properties of the femoral bone were modified according to Wang *et al.* [8]. Three different FE models were developed to represent different severities of osteoporosis in the femoral bone by reducing the values of both its Young's modulus and density by 10%, 20%, and 35%. As the majority of the load is carried by the cortical layer of the long bones [25,26], the present study assumes the mechanical contribution of the cancellous bone to be negligible and is assumed to be captured within the material description of the femoral cortical bone as detailed in this model. M_0 represented the FE model with the original (normal) material properties (elastic modulus) of the femur bone, M_1 with 10% reduction, M_2 with 20% reduction, and M_3 with 35% reduction in the elastic modulus value,

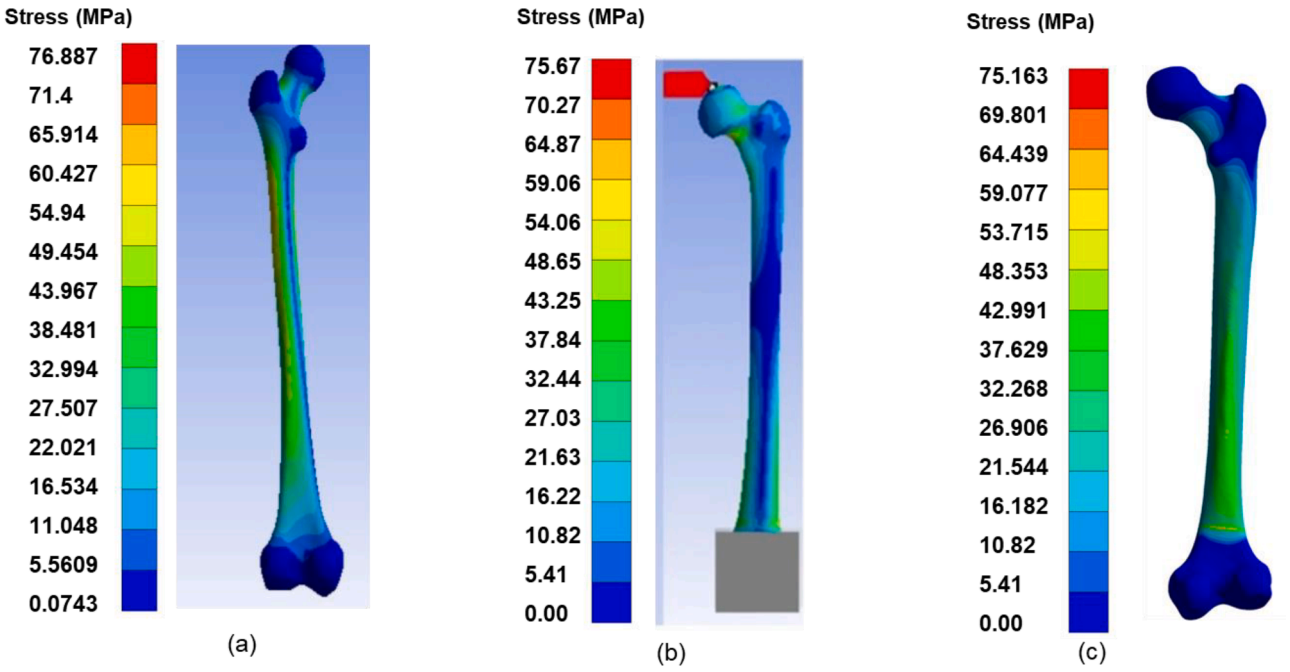

Fig. 5. Validation of the femur model with the previous literature. The equivalent stress distribution in the femur bone by Das et al. (2014), (b) Ebrahimi et al. (2012), and (c) present FE model.

respectively, reflecting the observed changes in osteoporotic bone. The load transfers through the fracture fixation assembly and AMTD before and after an osteoporosis-induced PFF was investigated.

2.5. Interface conditions

Contact analysis was performed to simulate the interaction between the femoral implant and bone, bone screws and bone, cables and bone, AMTD and bone, and all other fracture fixation assembly interfaces. Two extreme contact conditions were assumed for this analysis.

First, a non-bonded (non-osseointegration) condition was assumed at the interfaces between bone screws and bone cables to the bone and AMTD to the bone. While the fully bonded (osseointegration) condition was assumed between femoral implant and bone. Six-node surface-to-surface contact elements were used for the contact analysis. The coefficient of friction was defined as 0.2 for non-bonded interfaces [12]. Fully bonded contact conditions were applied to all other interfaces in the fracture fixation assembly.

In the second case, all of the interfaces were assumed to be fully bonded and an augmented contact algorithm was used to model this contact condition. For the convergence of non-linear solutions, a normal contact stiffness of 10 N/mm and a penetration factor of 0.1 were defined. Both the contact parameters (i.e., contact stiffness and penetration factor) were chosen so that they do not have any influence on the results.

2.6. Applied boundary and loading conditions

Initially, the femur model was analysed under standing posture loading and boundary conditions. In this case, the femur model was subjected to the different bodyweight loading conditions: 490 N, 540 N, 588 N, 640 N, and 860 N, in line with previously reported studies [27]. The loads corresponded to the different body weights (Table 2) [27]. The distal part of the femur bone was constrained in all degrees of freedom. The loading and boundary conditions for the standing posture are shown in Fig. 4 (a). Further, two physiological load cases approximating the peak loads through the stance phase of walking and stair climbing were also considered for the analysis. The normal walking loading condition comprised of the intersegmental and two joint muscle forces (I), abductor (A), tensor *fascia latae* proximal (TFL_p), tensor *fascia latae* distal (TFL_d), and *vastus laterallis* (VL) (Fig. 4 (b)). In comparison, the stair climbing loading condition comprised of the I, A, TFL_p, TFL_d, VL, and *vastus medialis* (VM) (Fig. 4 (c)). The distal part of the femur bone was fixed for both loading cases. Fig. 4 (b) and (c) illustrate the locations of the boundary and loading conditions for walking and stair climbing, respectively. The magnitude of each muscle and joint contact force was based on the assumed body weight of 860 N [16]. The magnitude and direction of all muscle and joint contact forces for both the physiological load cases were converted to our FE coordinate system (Table 3). These muscle and reaction forces were distributed on the set of nodes restrained to the respective patched areas. The location and insertion point of each muscle force was assigned according to Andreaus *et al.* [16].

3. Results

The intact FE model of the femoral bone was validated using metadata from studies by Ebrahimi *et al.* [24] and Das *et al.* [19] using the same material property data, boundary, and loading conditions. The results were in good agreement with the earlier published data. Fig. 5 shows the stress distribution in the femoral bone from previous studies and the present model. The highest von Mises stress was observed as 76.89 MPa in the femoral bone by Das *et al.* [19] and 75.67 MPa by Ebrahimi *et al.* [24]. The peak value of von Mises stress from the present model was 75.16 MPa in the femoral bone. It is postulated that the differences in the stress distributions were likely due to variations in the geometrical structures of the femoral bone between the three models.

3.1. Standing posture condition

The FE model was initially subjected to the standing posture loading condition at different body weights. The highest body weight (860 N) generated the greatest stresses and strains in all the components (Fig. 6). Although, the distribution pattern of the equivalent stresses and strains was similar for all the five body weight conditions (1-5) for the standing posture loading condition, the magnitudes of the stresses and strains

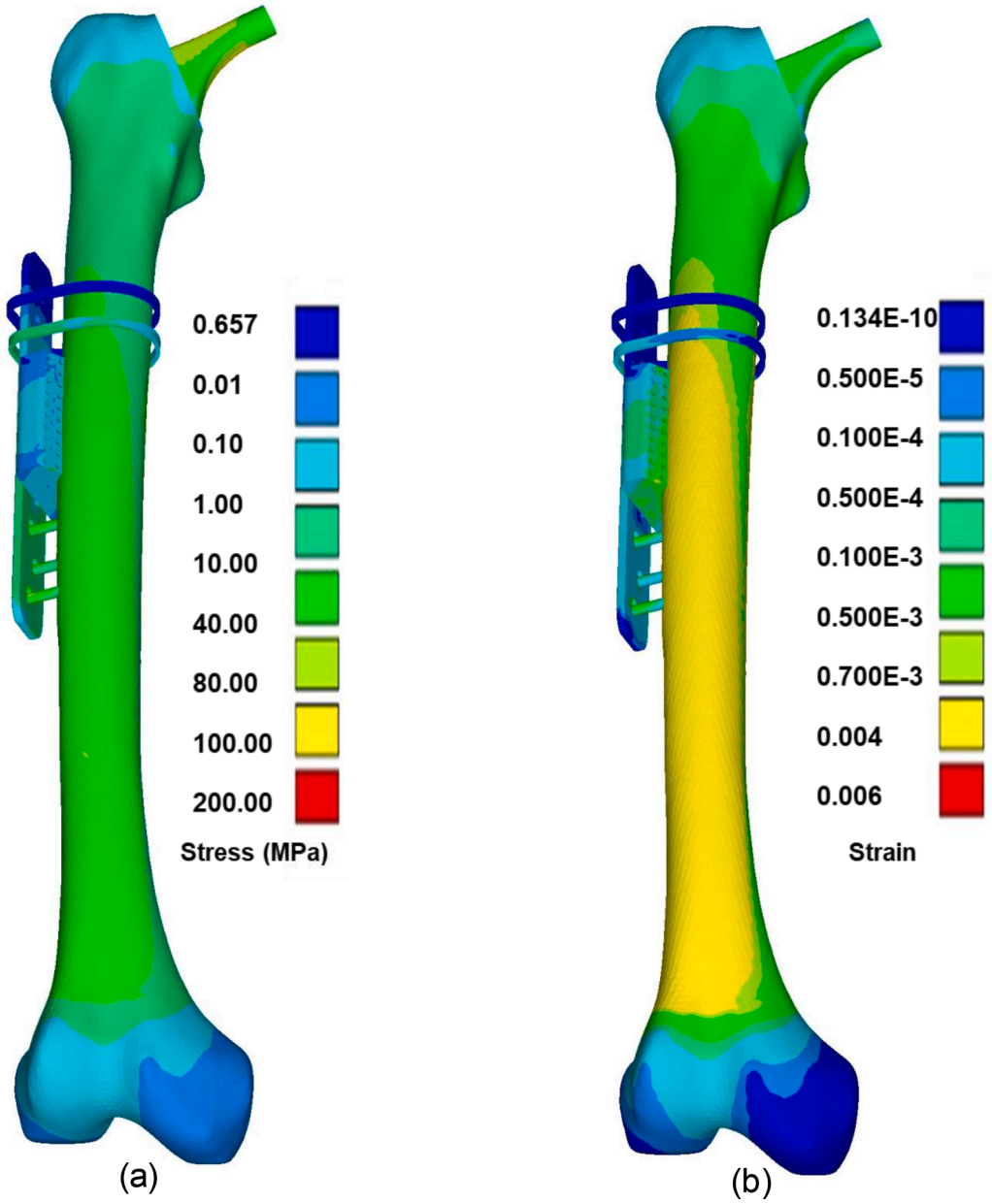

Fig. 6. (a) The equivalent stress distribution, and (b) equivalent strain distribution at the FE model of femur bone with fracture fixation assembly, AMTD, and femoral implant for the static loading condition of 860 N.

were markedly different (Fig. 8).

The von Mises stress distributions in the plate, femoral implant, AMTD, bone screw, femoral bone, cables, and cable holders for the 860 N non-bonded contact condition case are shown in Fig. 7 (a-g). Bone Screw 3 demonstrated the highest peak von Mises stress compared to all other components (Fig. 7 (d)), whereas Cable Holder 1 exhibited the lowest levels of von Mises stress (Fig. 7 (g)). Therefore, Bone Screw 3 was the main load-carrying component in the fixation assembly. The von Mises stress distributions in the plate, femoral implant, AMTD, bone screws, femoral bone, cables, and cable holders are shown in Fig. 7 (h-n) for the bonded condition. Compared with the non-bonded condition, the von Mises stress generally increased for all the components, except for the femoral bone, when the bonded contact conditions were applied. Although, the stress magnitudes are different, the stress distributions for all of the components were similar to the non-bonded condition.

The average von Mises stresses for the cable holders, cables, femoral implant, bone screws, AMTD, and plate for the body weight cases 1-5 (standing posture condition) for the non-bonded and bonded conditions are shown in Fig. 8. In the fracture fixation assembly, the average stress was higher at Bone Screw 3 followed by Bone Screw 1 and Bone Screw 2, the fracture fixation plate, cables, and cable holders for all load cases. For the non-bonded case, the average von Mises stress in Bone Screw 3 was 1.71 MPa, 5.01 MPa, 5.56 MPa, 6.15 MPa, and 9.01 MPa for load cases 1 to 5, respectively. Whereas, for the bonded condition the average von Mises stress was found to be 8.34 MPa, 25.72 MPa, 28.71 MPa, 31.02 MPa, and 34.01 MPa for Bone Screw 3 for load cases 1 to 5. The average von Mises stress values for all other components for the non-bonded and bonded conditions are presented in Fig. 8.

3.2. *Walking and stair climbing conditions*

The FE model was also used to model the stance phase of walking and stair climbing. Fig. 9 shows a comparison of the average von Mises stresses in the different components for standing, walking, and stair

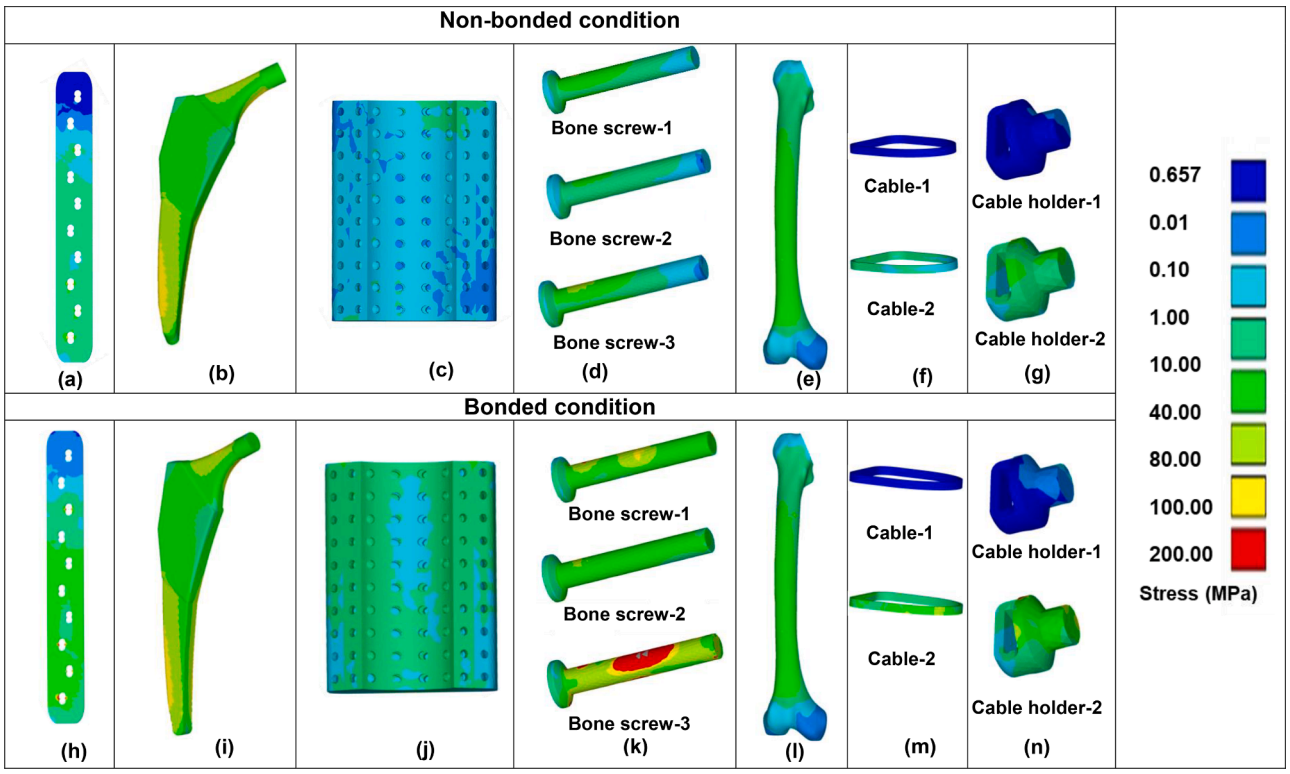

Fig. 7. The equivalent stress distribution in the (a) plate, (b) femoral implant, (c) AMTD, (d) bone screws, (e) femur, (f) cables, (g) cable holders for non-bonded and (h) plate, (i) femoral implant, (j) scaffold device, (k) bone screws, (l) femur, (m) cables, (n) cable holders for bonded conditions of the FE model subjected to the static load of 860 N.

climbing conditions. The stair climbing demonstrated higher values of average stresses for all the components compared to standing and walking conditions. Similar to the standing loading condition, the highest stress was observed in Bone Screw 3 in the fracture fixation assembly for walking and stair climbing. However, the average von Mises stress value for Bone Screw 2 was less for the walking loading condition compared to the standing and stair climbing loading conditions. The peak von Mises stresses in the AMTD device were 4.20 MPa, 9.22 MPa, and 25.77 MPa for standing, walking, and stair climbing loading conditions. The AMTD was found to be within the safe limit (below the yield strength for the PLLA/PCL/PHBV blend of 53 MPa) when tested under all three physiological loading conditions.

In the case of the osteoporotic models, the average stress distribution in the femoral bone, AMTD, and bone screws due to different material modelling of the bone (i.e., 0% (M_0), 10% (M_1), 20% (M_2), and 35% (M_3) reduction in bone material property data), is shown in Fig. 10. The lowest average stress in the femoral bone was found for model M_3, followed by M_2, M_1, and M_0 (Fig. 10). The reduction in the average stress value was found to be 0.9%, 1.78%, and 3.45% for M_3, M_2, and M_1. A decrease of stress in the femoral bone would increase the load transfer at the fixation assembly. The reduction of the elastic modulus values for the femoral bone corresponding to the severity of osteoporosis led to an increase in the average stress values for all three bone screws (Fig. 10). The highest stress value for all bone screws was found in model M_3. Similarly, a concomitant increase in the peak von Mises stress value in the AMTD was also observed due to the reduction of the material property data of the femoral bone. The maximum von Mises stress of 6.93 MPa was found for the AMTD in the M_3 model. The equivalent stress distribution at the bone screws and AMTD for models M_0, M_1, M_2, and M_3 are shown in Fig. 11. The FE model for M_3 exhibited the highest stress distribution for all the bone screws and AMTD compared with other FE models M_0, M_1, and M_2 (Fig. 11).

3.3. *Effect of fracture fixation assembly material*

The effect of the fracture fixation material on the stress distribution within the FE model's components (i.e., plate, cables, cable holders, and bone screws) was also investigated. The equivalent stress distributions in all the fracture fixation assembly components for different materials is shown in Fig. 12. The choice of material (i.e., stainless steel (SS316L), alumina (Al_2O_3), cobalt chrome (Co-Cr) alloy, or titanium alloy (Ti-6Al-4V)) had a negligible effect on the stress distributions in the AMTD, femoral implant, and femoral bone. The stress distributions were found similar in the AMTD, femoral implant, and femur bone for the different fixation materials investigated. However, the different fixation material property data influenced the stress distributions at the plate, cables, cable holders, and bone screws. The stresses in the plates, cables, cable holders, and bone screws were minimised when Ti-6Al-4V alloy was used for the fracture fixation assembly compared to the other materials investigated (SS316L, Al_2O_3, Co-Cr based alloys) (Fig. 12).

4. Discussion

PPF of the long bones has high incidence in older patients following a total hip replacement and is a significant socio-economic problem with 18% of total hip replacements resulting in PPF [5]. A novel concept was proposed to attach an AMTD using existing fracture fixation solutions to the compact outer layer of the bone at the fracture site to stimulate bone regeneration. The aim of this study was to develop a 3D FE model of the AMTD with a fracture fixation assembly attached to the femoral bone and simulating different physiological loading conditions to determine whether or not the stresses within the AMTD were below the material's fracture strength. The primary function of the AMTD was to enhance fracture healing through the controlled delivery of bone-regulating molecules, while conventional fracture fixation solutions sustain the physiological loads and prevent mechanical failure during the bone

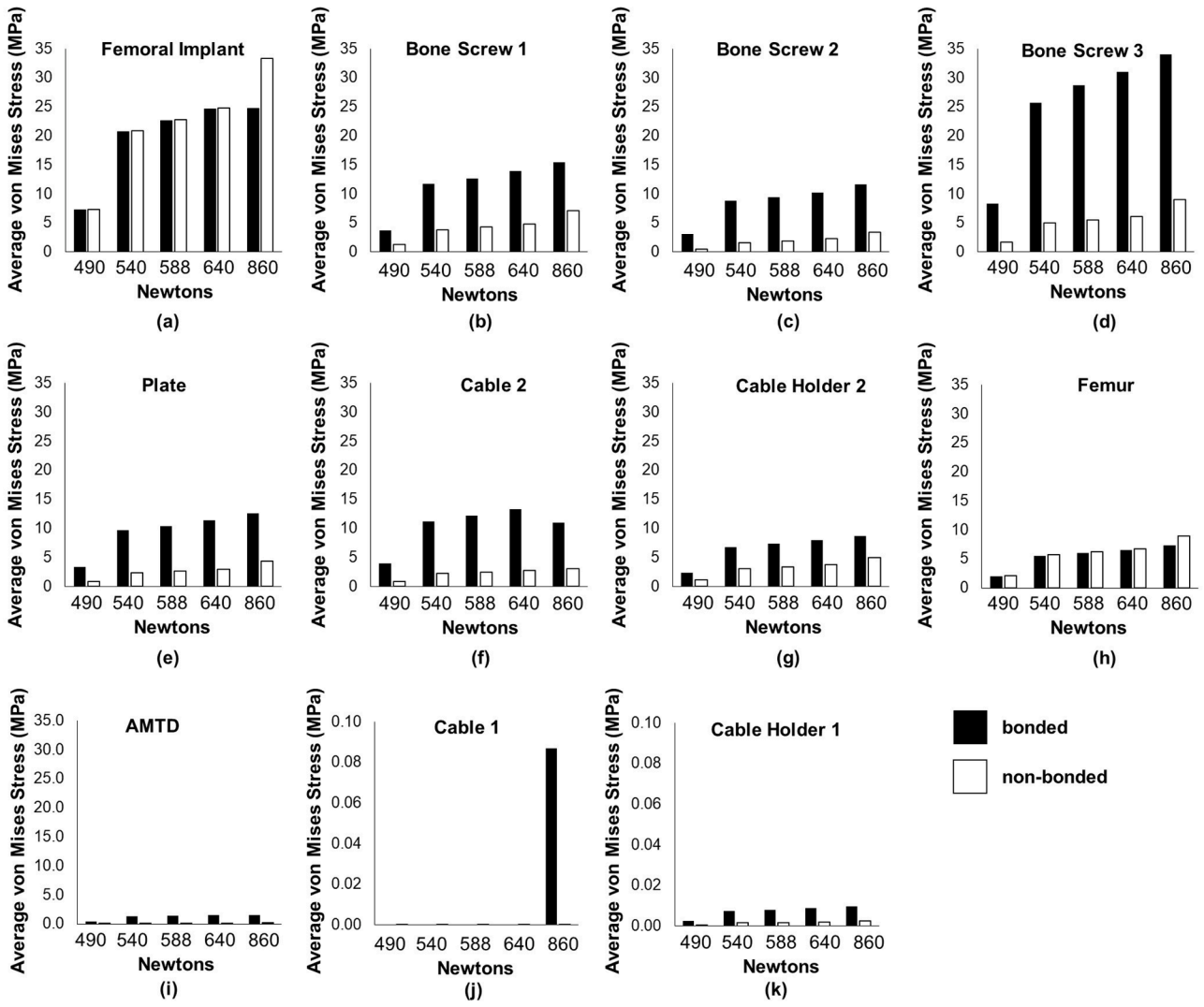

Fig. 8. The average equivalent stresses in the (a) femoral implant, (b) bone screw 1, (c) bone screw 2, (d) bone screw 3, (e) plate, (f) cable 2, (g) cable holder 2, (h) femur, (i) AMTD, (j) cable 1, and (k) cable holders 1 of FE model for the non-bonded and bonded conditions during the standing posture of different load cases, i.e., Load case 1: 490 N, Load case 2: 540 N, Load case 3: 588 N, Load case 4: 640 N, and Load case 5: 860 N.

regeneration process.

The 3D FE model was initially subjected to a standing posture loading condition for different body weights. As expected, the highest body weight value (860 N) showed the highest stresses at all the components. Approximately 70-80% of the load was transferred through the fracture fixation assembly compared to the other components. These results are in agreement with the earlier FE studies of femoral fracture fixation plate assemblies that show load distribution in the bone-plate interface, primarily supported by plates and bone screws [22,28–32]. We observed the bone screws in the fracture fixation assembly were the main load-carrying components for the present model. The highest stress distribution was found in Bone Screw 3 (Fig. 7). Previously, it has been reported that the bone screws carried the maximum load and play an important role for the success of the fixation device in the treatment of osteoporotic fractures [33]. The cable holders had the lowest values of stress of all the components (Fig. 7). The AMTD was found to be within the safe limit (i.e., below the yield strength of PLLA/PCL/PHBV blend of 53 MPa) [17] for all three physiological loading conditions. Previous work suggests that complete osseointegration between the bone screws and cables and bone benefits long-term performance [34–37].

The stair climbing physiological loading exhibited during the stance phase of gait generated higher stresses for all the components of the FE model compared to the other two physiological loading conditions, i.e., walking and standing (Fig. 9). During the stair climbing, the peak load of the muscle and reaction forces was higher compared to the walking, corresponding to an increment in the stress values [16]. Although, in a realistic scenario, stair climbing for a patient having PPF is a very challenging task. In reality, it is assumed that patient having PPF is not subjected to the stair climbing loading condition very often. In this study, the osteoporotic bone was represented by the reduction in the material property similar to earlier studies [8,19,38,39]. As the maximum load is carried by the outer cortex or cortical bone in the femur, the present study only focused on the femoral cortical bone. Osteoporotic bone results in a decrease in the pull-out strength and shearing strength [40]. The reduction of density and material value leads to the reduction of load transfer at the femur bone. This study clearly demonstrates that the AMTD and standard fixation solutions sustain the physiological loads and avoid mechanical failure.

Biomaterials play an important role in the efficacy of fixation plates because of their direct and indirect effects on the healing process [20]. Various biomaterials such as, titanium, titanium alloys (Ti-6Al-4V), stainless steel (SS316L), cobalt-chromium (Co-Cr) alloys and ceramics (Al_2O_3) have been used in the orthopaedic industry [41]. Herein, we have investigated the mechanical aspect of key biomaterials for the long-term success of present fixation assemblies. To achieve this the present study investigated the effect of the different material properties

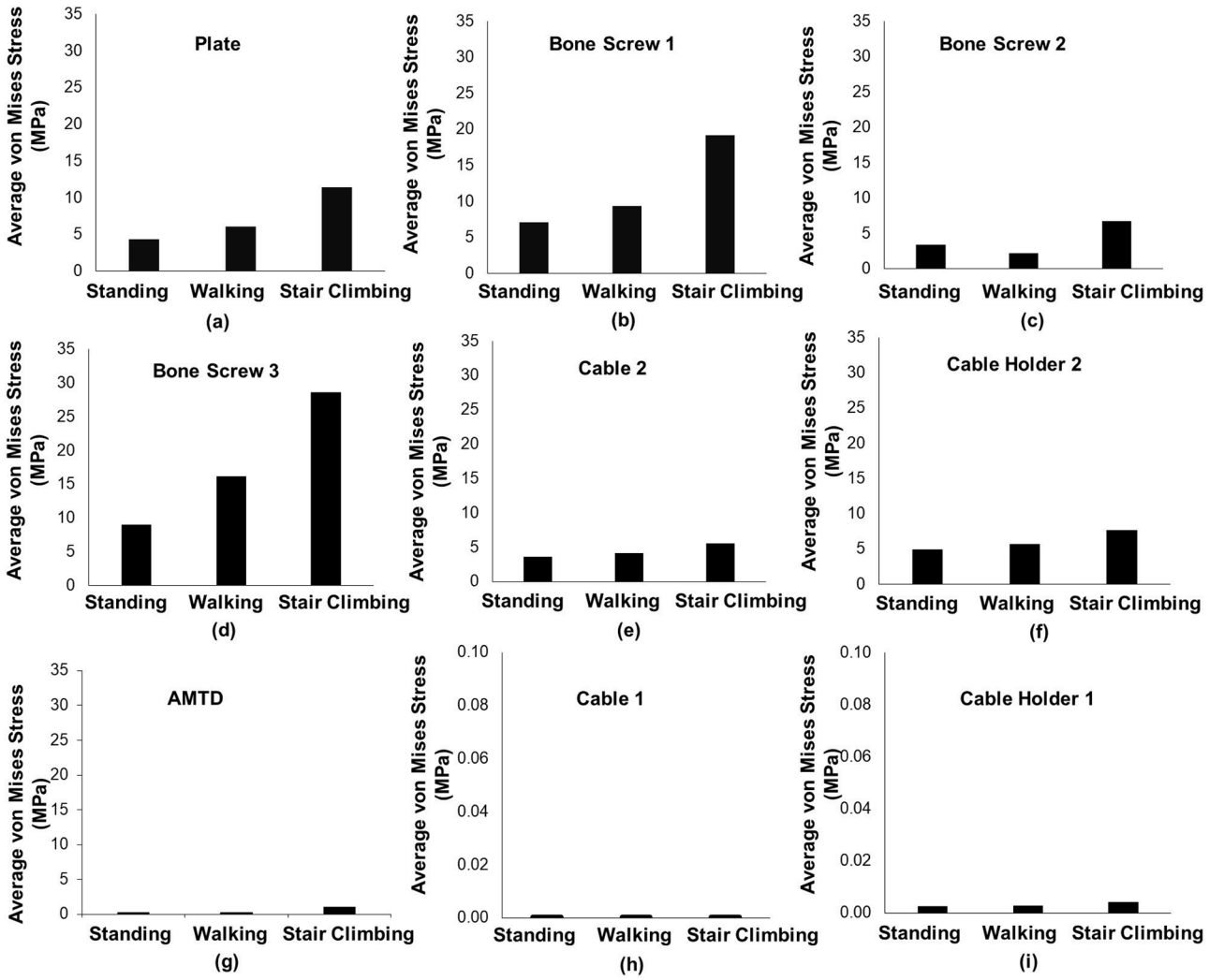

Fig. 9. The average equivalent stresses in the (a) plate, (b) bone screw 1, (c) bone screw 2, (d) bone screw 3, (e) cable 2, (f) cable holder 2, (g) AMTD, (h) cable 1, and (i) cable holder 1 of the FE model for standing, stair climbing, and walking condition.

of fracture fixation assembly on the stress distribution. Here, the fixation assembly (*i.e.,* metallic fixation plates, bone screws, cables, and cable holders) was assigned with different materials such as alumina Al_2O_3, Co-Cr alloy, SS316L, and Ti-6Al-4V. However, the components of fixation assembly showed variations in stress distribution due to different materials. For example, the bone screws had a smaller stress value for the material combination of Ti-6Al-4V compared to the other materials. At present, the bone plates for internal and external fixation generally used in the clinic are primarily made of stainless steel and Ti-6Al-4V [42–44]. It has previously been demonstrated in the studies of different biomaterials for the fracture fixation plates and screws that stresses at the bone plates and screws were found to be less for Ti-6Al-5V compared to SS316L and Co-Cr [19]. The present results are in agreement with the previous outcomes. Therefore, the Ti-6Al-4V material can be used for the fixation assembly for long-term performance and significantly reduces the risk of failure of the fixation assembly components.

While the FE model presented here clearly demonstrates the ability of the fracture fixation assembly to divert loading away from the AMTD, some limitations remain that should be addressed in future work. Periosteal tissues were omitted from the model as it was assumed that the material properties of these soft tissues are significantly less than bone [26,27], and that they do not have a significant effect of the stress distribution within the femur bone and fracture fixation assembly. It should also be noted that the FE model described here is based on a single CT scan dataset that is useful for patient-specific models, devices, and tailored rehabilitation programmes. Whilst, a morphologically averaged model of the femur bone developed from CT scans of multiple persons would provide a more generalised understanding of the biomechanics at play during the loading conditions investigated here. Both approaches provide value for engineers and medical professions and should be investigated synergistically to obtain a complete understanding of the biomechanics. Further, the material properties of cortical bone were assigned to the entire femur considering that the majority of the load is transferred through the outer cortical layer of the bone and not the cancellous bone [22,23,26]. Bone fracture was not explicitly modelled in these FE models as it was assumed that the fracture gap has been closed by the fracture fixation plate in the non-osseointegrated boundary condition, and that the fracture gap has been closed and fusion has occurred in the osseointegrated loading condition. Finally, the AMTD material properties used here were derived from the bulk material. However, the AMTD was fabricated using FDM 3D printing and possesses anisotropic mechanical properties that may result in different stress values for the AMTD device. Future work will characterise the mechanical behaviour of the FDM 3D printed material.

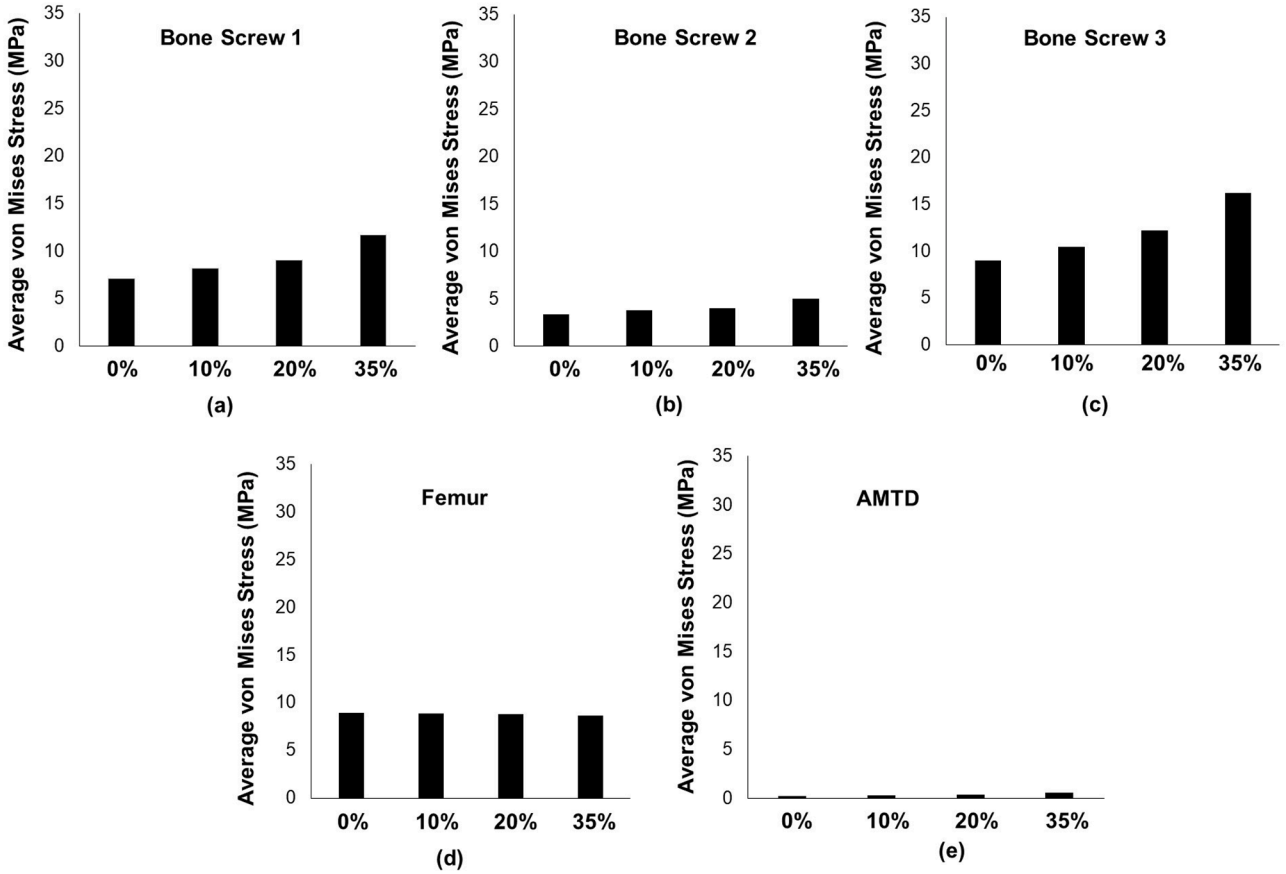

Fig. 10. The average von Mises stress distribution in the (a) bone screw 1, (b) bone screw 2, (c) bone screw 3, (d) femur, and (e) AMTD due to the material reduction at the femur bone in case of the non-bonded condition.

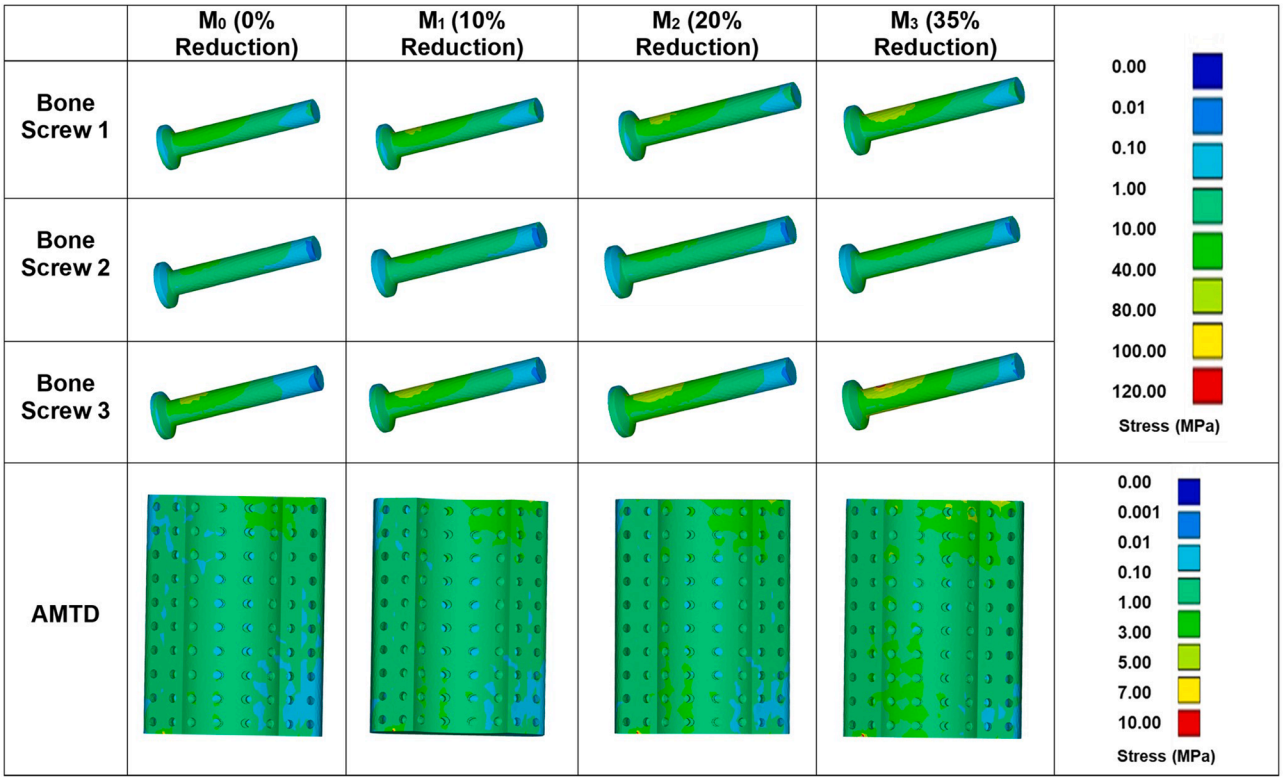

Fig. 11. The equivalent stress distribution in the bone screws and AMTD due to the reduction of material property at the femur bone in case of the non-bonded condition.

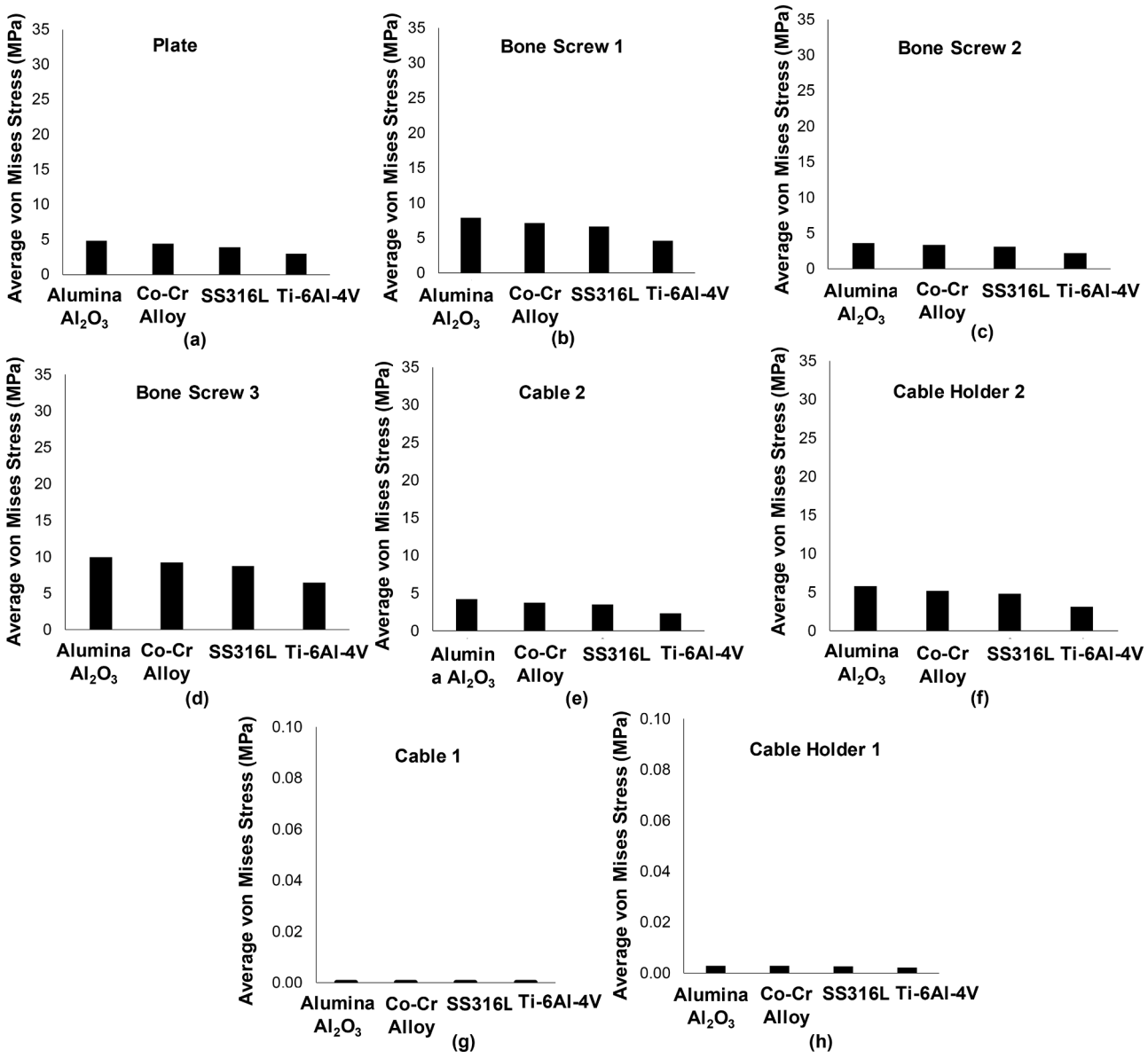

Fig. 12. The average von Mises stress distribution in the (a) plate, (b) bone screw 1, (c) bone screw 2, (d) bone screw 3, (e) cable 2, (f) cable holder 2, (g) cable 1, and (h) cable holder 1 of the FE model for the different material properties of the fracture fixation assembly.

5. Conclusion

The current study concluded that the proposed polymeric-based AMTD was non-load bearing. The maximum load during standing, walking, and stair climbing was carried by the fracture fixation assembly with the bone screws carrying the bulk of the load. The peak stress values within the AMTD for the standing, walking, and stair climbing loading conditions were approximately 8%, 17%, and 49% of the yield strength of the PLLA/PCL/PHBV AMTD. Therefore, the mechanical design of the AMTD has been validated. It can be also concluded that the use of Ti-6Al-4V for the fracture fixation assembly could improve long-term performance.

Ethical approval

Not required.

Declaration of Competing Interest

The authors declared no potential conflicts of interest concerning this article's research, authorship, and publication.

Acknowledgments

This study is supported by the European Union's Horizon 2020 Research and Innovation programme under grant agreement No 814410: GIOTTO: Active aGeIng and Osteoporosis: The next challenge for smarT nanobiOmaterials and 3D technologies. Additionally, the CT data used in this study were generated by the National Cancer Institute Clinical Proteomic Tumor Analysis Consortium (CPTAC).

References

[1] Souza T, Ozisik L, Basaran NC. An overview and management of osteoporosis. Eur J Rheumatol 2017;4:46–56.
[2] Hernlund E, Svedbom A, Ivergard M, Compston J, Copper C, Stenmark J, McCloskey EV, Jönsson B, Kanis JA. Osteoporosis in the European Union: medical management, epidemiology and economic burden. A report prepared in

collaboration with the International Osteoporosis Foundation (IOF) and the European Federation of Pharmaceutical Industry Associations (EFPIA). Arch Osteopor 2013;8(1):136.
[3] Franklin J, Malchau H. Risk factors for periprosthetic femoral fracture. Injury 2007;38(6):655–60.
[4] Marsland D, Mears SC. A review of periprosthetic femoral fractures associated with total hip arthroplasty. Geriatr Orthopaed Surgery Rehab 2012;3(3):107–20.
[5] Capone A, Congia S, Civinini R, Marongiu G. Periprosthetic fracture: epidemiology and current treatment. Clin Cases Mineral Bone Metab 2017;14(2):189–96.
[6] Drew JM, Griffin WL, Odum SM, Doren BV, Weston BT, Stryker LS. Survivorship after periprosthetic fracture: factors affecting outcome. J Arthropl 2016;31:1283–8.
[7] Bhattacharya T, Chang D, Meigs JB, Estook DM, Malchau H. Mortality after periprosthetic fracture of the Femur. J Bone Joint Surgery 2007;89(12):2658–62.
[8] Wang G, Wang D, Mao J, Lin J, Yin Z, Wang B, He Y, Sun S. Three dimensional finite-element analysis of treating Vancouver B1 periprosthetic femoral fractures with three kinds of internal fixation. Int J Clin Experim Med 2016;9(4):7557–64.
[9] Pandithevan P, Kumar GS. Finite element analysis of a personalized femoral scaffold with designed microarchitecture. Proc IMechE, Part H: J Eng Med 2010;224:877–89.
[10] Almeida HA, Bartolo PJ. Topological optimisation of scaffolds for tissue engineering. Proc Eng 2013;59:298–306.
[11] Adachi T, Osako Y, Tanaka M, Hojo M, Hollister SJ. Framework for optimal design of porous scaffold microstructure by computational simulation of bone regeneration. Biomaterials 2006;27:3964–72.
[12] Mondal S, Ghosh R. Experimental and finite element investigation of total ankle replacement: A review of literature and recommendations. J Orthopaed 2020;18:41–9.
[13] Melo P, Naseem R, Corvaglia I, Montalbano G, Pontremoli C, Azevedo A, Quadros P, Gentile P, Ferreira AM, Dalgarno K, Vitale-Brovarone C, Fiorilli S. Processing of Sr^{2+} containing poly L-lactic acid-based hybrid composites for additive manufacturing of bone scaffolds. Front Mater 2020;7:601645.
[14] National Cancer Institute Clinical Proteomic Tumor Analysis Consortium (CPTAC). (2018). Radiology Data from the Clinical Proteomic Tumor Analysis Consortium Sarcomas [CPTAC-SAR] collection [C3N-00875]. The Cancer Imaging Archive. DOI: 10.7937/TCIA.2019.9bt23r95.
[15] Clark K, Vendt B, Smith K, Freymann J, Kirby J, Koppel P, Moore S, Phillips S, Maffitt D, Pringle M, Tarbox L, Prior F. The cancer imaging archive (TCIA): maintaining and operating a public information repository. J Digit Imag 2013;26(6):1045–57. Dec.
[16] Andreaus U, Colloca M. Prediction of micromotion initiation of an implanted femur under physiological loads and constraints using the finite element method. Proc IMechE, Part H: J Eng Med 2009;223:589–605.
[17] Naseem R, Montalbano G, German MJ, Ferreira AM, Gentile P, Dalgarno K. Influence of PCL and PHBV on PLLA thermal and mechanical properties in binary and ternary polymer blends. Molecules 2022;27:7633.
[18] Sensoy AT, Colak M, Kaymaz I, Findik F. Optimal material selection for total hip implant: A finite element case study. Arab J Sci Eng 2019;44:10293–301.
[19] Das S, Sarangi SK. Finite element analysis of femur fracture fixation plates. Int J Basic Appl Biol 2014;1:1–5.
[20] Deshmukh RM, Kulkarni SS. A review on biomaterials in orthopaedic bone plate application. Int J Curr Eng Technol 2015;5(4):2587–91.
[21] Maharaja PSRS, Maheswaranb R, Vasanthanathana A. Numerical analysis of fractured femur bone with prosthetic bone plates. Proc Eng 2013;64:1242–51.
[22] Dhanopia A, Bhargava M. Finite element analysis of human fractured femur bone implantation with PMMA thermoplastic prosthetic plate. Proc Eng 2017;173:1658–65.
[23] Gouda AT, Jagadish SP, Dinesh KR, Gouda V, Prashant N. Characterization and investigation of mechanical properties of hybrid natural fiber polymer composite materials used as orthopaedic implants for femur bone prosthesis. J Mechan Civil Eng 2014;11:40–52.
[24] Ebrahimi H, Rabinovich M, Vuleta V, Zalcman D, Shah S, Dubov A, Roy K, Siddiqui FS, Schemitsch EH, Bougherara H, Zdero R. Biomechanical properties of an intact, injured, repaired, and healed Femur: An experimental and computational study. J Mech Behav Biomed Mater 2012;16:121–35.
[25] Mondal S, Ghosh R. A numerical study on stress distribution across the ankle joint: Effects of material distribution of bone, muscle force and ligaments. J Orthopaed 2017;14(3):329–35.
[26] Mondal S, Ghosh R. Effects of implant orientation and implant material on tibia bone strain, implant-bone micromotion, contact pressure, and wear depth due to total ankle replacement. IMechE, Part H: J Eng Med 2019;233(3):318–31.
[27] Mathukumar S, Nagarjan VA, Radhakrishnan A. Analysis and validation of femur bone data using finite element method under static load condition. IMechE, Part C: J Mechan Eng Sci 2019;223(16):5547–55.
[28] Tamimi AA, Quental C, Folgado J, Peach C, Bartolo P. Stress analysis in a bone fracture fixed with topology-optimised plates. Biomech Modell Mechanobiol 2020;19:693–9.
[29] Kata NM, Abidin NAZ, Aziz AUA, Abdullah AH, Wui NB, Nasution AK, Kadir MRA, Ramlee MH. Finite element analysis of external fixator for treating femur fracture: analysis on stainless steel and titanium as material of external fixator. Malaysian J Fundam Appl Sci 2021;17:274–84.
[30] Huang X, Zhi Z, Yu B, Chen F. Stress and stability of plate-screw fixation and screw fixation in the treatment of Schatzker type IV medial tibial plateau fracture: A comparative finite element study. J Orthopaed Surg Res 2015;10:182.
[31] Terzini M, Aldieri A, Nurisso S, Nisco GD, Bignardi C. Finite element modelling application in forensic practice: A periprosthetic femoral fracture case study. Front Bioeng Biotechnol 2020;8:1–11.
[32] Wang K, Kenanidia E, Miodowink M, Tsirdis E, Moazen M. Periprosthetic fracture fixation of the femur following total hip arthroplasty: A review of biomechanical testing- Part II. 2019; 61: 144-162.
[33] Seebeck J, Goldhahn J, Morlock MM, Schneider E. Mechanical behavior of screws in normal and osteoporotic bone. Osteoporos Int 2005;16(2):107–11.
[34] Mondal S, Ghosh R. The effects of implant orientations and implant–bone interfacial conditions on potential causes of failure of tibial component due to total ankle replacement. J Med Biol Eng 2019;39:541–51.
[35] Mondal S, Ghosh R. Influence of cancellous bone material and dead zone on stress-strain, bone stimulus and bone remodelling around the tibia for total ankle replacement. IMechE, Part H: J Eng Med 2021;235:185–96.
[36] Ghosh R, Gupta S. Bone remodelling around cementless composite acetabular components: The effects of implant geometry and implant-bone interfacial conditions. J Mech Behav Biomed Mater 2014;32:257–69.
[37] Mondal S, Ghosh R. Bone remodelling around the tibia due to total ankle replacement: effects of implant material and implant–bone interfacial conditions. Comput Methods Biomech Biomed Eng 2019;22:1247–57.
[38] Peng Y, Du X, Huang L, Li J, Zhan R, Wang W, Xu B, Wu S, Peng C, Chen S. Optimizing bone cement stiffness for vertebroplasty through biomechanical effects analysis based on patient-specific three-dimensional finite element modelling. Med Biol Eng Comput 2018 Nov;56(11):2137–50.
[39] Wang D, Li Y, Yin H, Li J, Qu J, Jiang M, Tian J. Three-dimensional finite element analysis of optimal distribution model of vertebroplasty. Ann Palliat Med 2020;9(3):1062–72.
[40] Shea TM, Jake Laun J, Gonzalez-Blohm SA, Doulgeris JJ, Lee WE, Aghayev K, Vrionis FD. Designs and Techniques That Improve the Pullout Strength of Pedicle Screws in Osteoporotic Vertebrae: Current Status. 2014; 1-15.
[41] Tapscott DC, Wottowa C. Orthopedic implant materials. 2022 Jul 25. StatPearls [Internet]. Treasure Island (FL): StatPearls Publishing; 2022. Jan–. PMID: 32809340.
[42] Saini M, Singh Y, Arora P, Arora V, Jain K. Implant biomaterials: a comprehensive review. World J Clin Cases 2015;3(1):52–7.
[43] Mitsuo N, Yi L, Masaki N, Huihong L, Hua L. Biomedical titanium alloys with Young's moduli close to that of cortical bone. Regener Biomater 2016;3:173–85.
[44] Voggenreiter G, Leiting S, Brauer H, Leiting P, Majetschak M, Bardenheuer M, Obertacke U. Immuno-inflammatory tissue reaction to stainless-steel and titanium plates used for internal fixation of long bones. Biomaterials 2003;24:247–54.